2020 1st International Conference on Information Technology, Advanced Mechanical and Electrical Engineering (ICITAMEE) | 978-1-7281-8309-1/20/$31.00 ©2020 IEEE | DOI: 10.1109/ICITAMEE50454.2020.9398392

COVID-19Net: A Deep Neural Network for COVID-19 Diagnosis via Chest Radiographic Images

1st Dhimas Arief Dharmawan
Department of Electrical Engineering
Universitas Muhammadiyah Yogyakarta
Bantul, Indonesia
email: dhimasariefdharmawan@umy.ac.id

2nd Latifah Listyalina
Department of Electrical Engineering
Universitas Respati Yogyakarta
Sleman, Indonesia
email: listyalina@respati.ac.id

***Abstract*—Recently, Corona Virus Disease 2019 (COVID-19) has rapidly spanned the globe. In particular, this viral disease has infected more than 400,000 peoples and has caused more than twenty thousand cases of death. Unfortunately, there is no specific therapeutic drugs or vaccines for the disease, such that an early screening protocol is highly required. Although nucleic acid detection using real-time polymerase chain reaction (RT-PCR) remains the standard, recent literature reported that radiological imaging of human chests had shown a more consistent result when used for COVID-19 diagnosis. However, performing a manual evaluation on chest computed tomography or CXR images is tedious and labour-extensive. In this paper, we present COVID-19Net, a deep neural network-based algorithm to assist doctors in diagnosing COVID-19 through the radiographic images. In the experimental parts, our algorithm could diagnose COVID-19 and other related diseases like SARS, Streptococcus, ARDS, and Pneumocystis with average accuracy and area under the ROC curve (AUC) of $> 99\%$ and > 0.99, respectively.**

***Index Terms*—COVID-19, CXR images, deep learning, diagnosis.**

I. Introduction

In early of 2020, the World Health Organization (WHO) has declared COVID-19 to be a global health emergency. This disease has spread across the world and has led to more than twenty thousand cases of death. Unfortunately, specific therapeutic drugs or vaccines for the disease has not been found, such that an early screening protocol is highly required. Although nucleic acid detection using real-time polymerase chain reaction (RT-PCR) remains the standard, recent literature reported that radiological imaging of human chests is useful for COVID-19 diagnosis [1]–[3].

Although radiological imaging has shown a promising result in COVID-19 diagnosis, manual evaluations on chest computed tomography or CXR images by doctors are tedious, time-consuming, and labour-extensive. Moreover, to the best of our knowledge, no research presents an algorithm for the automatic diagnosis of COVID-19 from radiological images. In this paper, we propose COVID-19Net, a deep neural network-based algorithm to assist doctors in diagnosing COVID-19 through the chest radiographic (CXR) images. To build the algorithm, we tailor the DenseNet-121 architecture to the COVID-19 and other related diseases like SARS, Streptococcus, ARDS, and Pneumocystis characteristics. In the experimental parts, our algorithm could diagnose COVID-19 and other associated pathologies with average accuracy and area under the ROC curve (AUC) of $> 99\%$.

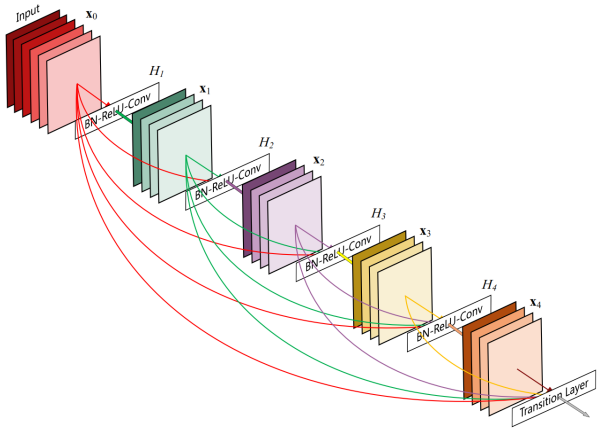

Fig. 1: DenseNet with 5 layers and the growth rate of $k = 4$ [4].

We organize the remaining sections of this paper as follows. Section II describes the details of the proposed COVID-19Net. In this section, we also describe the data and training procedures. In Section III, we present and discuss the experimental results. Finally, Section IV provides a concluding remark and recommendations for future work.

II. Methodology

In this section, we describe the details of our proposed methodology by initially providing a brief introduction to several deep neural network architectures. Subsequently, we present the configuration of COVID-19Net, followed by explanations on the training procedures and CXR images.

A. Densely Connected Convolutional Networks

Deep neural networks have attained significant improvements compared to the state-of-the-art machine learning algorithms in many tasks. These include object recognition [5]–[7], image classification [8]–[11], and image segmentation [12]–[18]. These successes are mainly due to the utilized multiple layers to capture the features of input data. This fact

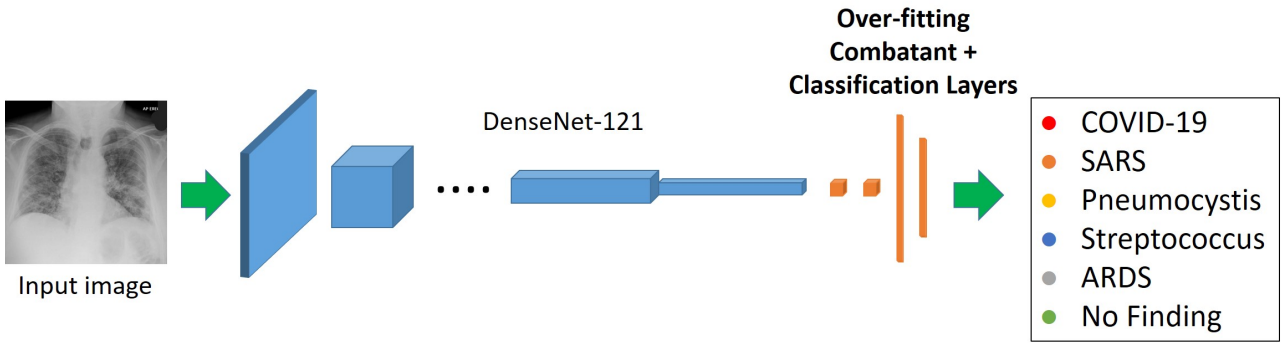

Fig. 2: The schematic diagram of our proposed algorithm.

suggests that the developments of deeper networks for better recognition, classification, and segmentation performance.

Although deeper networks may be useful to capture more features of the input data, the realization procedure is not straightforward, i.e., by solely stacking more layers to the network. As reported by several works in the literature, solely stacking a large number of layers to build a deeper neural network is prone to a vanishing gradient problem [4], [19], [20]. When the number of layers increases, the path for the information and gradient are getting longer. Hence, the information from the input layer or the gradient from the opposite side could get vanished before they reach the other side.

Recently, there exist several deep networks, such as Residual Neural Networks (ResNets) and Densely Connected Convolutional Networks (DenseNets), proposed to tackle the vanishing gradient problem. In general, such networks apply particular connectivity patterns to maximise the information and gradient flow. ResNets do the job by utilising skip connections that allow the information and gradient to jump over some layers. The models have successfully surpassed the performance of the preceding models, such as AlexNet [8] and VGG16 [11] in the image classification task with fewer training parameters.

The skip connections concept has instigated the development of the dense connectivity pattern used in DenseNets [4]. Unlike the skip connection that let the information to jump only over some layers, the dense connectivity pattern allows any layer in DensNets to connect with all subsequent layers. As a result, the l^{th} layer in DenseNets would take the feature maps of the preceding layers, $x_0, \ldots, x_{l-1}$, as the input:

$$x_l = H_l\left([x_0, x_1, \ldots, x_{l-1}]\right), \tag{1}$$

where $H_l\left(.\right)$ refers to any composite function of operations like batch normalization (BN). Figure 1 illustrates the layout of DenseNets with five layers and the expanding factor of $k = 4$. The connectivity pattern of DenseNet helps this model to solve the vanishing gradient problem. Also, since layers in DenseNets are very narrow, it would require fewer parameters compared to those of ResNets.

B. COVID-19Net

Developing an algorithm for COVID-19 diagnosis is a very challenging task. In particular, the algorithm should satisfy at least three aspects as follows. First, the developed algorithm should have a high rate of accuracy. Second, the algorithm should have a satisfactory generalization ability. Finally, since it is intended for broad early screening instruments, the algorithm should not lead to any computational problem.

TABLE I: The configuration of COVID19-Net.

Layers	Output Size	Operations
Input	224×224	
Convolution	112×112	7×7 conv, stride 2
Pooling	56×56	3×3 max pool, stride 2
Dense Block (1)	56×56	$\begin{bmatrix} 1 \times 1 \text{ conv} \\ 3 \times 3 \text{ conv} \end{bmatrix} \times 6$
Transition Layer (1)	56×56	1×1 conv
	28×28	2×2 average pool, stride 2
Dense Block (2)	28×28	$\begin{bmatrix} 1 \times 1 \text{ conv} \\ 3 \times 3 \text{ conv} \end{bmatrix} \times 12$
Transition Layer (2)	28×28	1×1 conv
	14×14	2×2 average pool, stride 2
Dense Block (3)	14×14	$\begin{bmatrix} 1 \times 1 \text{ conv} \\ 3 \times 3 \text{ conv} \end{bmatrix} \times 24$
Transition Layer (3)	14×14	1×1 conv
	7×7	2×2 average pool, stride 2
Dense Block (4)	7×7	$\begin{bmatrix} 1 \times 1 \text{ conv} \\ 3 \times 3 \text{ conv} \end{bmatrix} \times 16$
Pooling	1×1	7×7 global average pool
Over-fitting Combatant Layer	1×1	drop-out, 0.5 drop-out rate
		Batch Normalization (BN)
Classification Layer		6D fully connected layer, softmax

In general, deep neural networks would satisfy the first requirement. However, to have a good generalization ability, most deep neural networks would render a large number of data and a very deep architecture. As a result, most deep networks would lead to computational problems. As pointed out by [4], DenseNets could achieve better classification results than their counterparts on the ImageNet dataset with fewer parameters. Hence, DenseNets would be an ideal solution for the COVID-19 diagnosis algorithm. Moreover, using DenseNets, we could build a very deep network without causing vanishing gradient problems.

Figure 2 shows the schematic diagram of our proposed algorithm for COVID-19 diagnosis. As shown in the figure, we build an algorithm for COVID-19 diagnosis by tailoring DenseNet-121 to the COVID-19 and other related diseases characteristics. For the easiness of referencing, from now on, we call the developed algorithm as COVID-19Net. Table I shows the configuration of COVID-19Net. Similar to

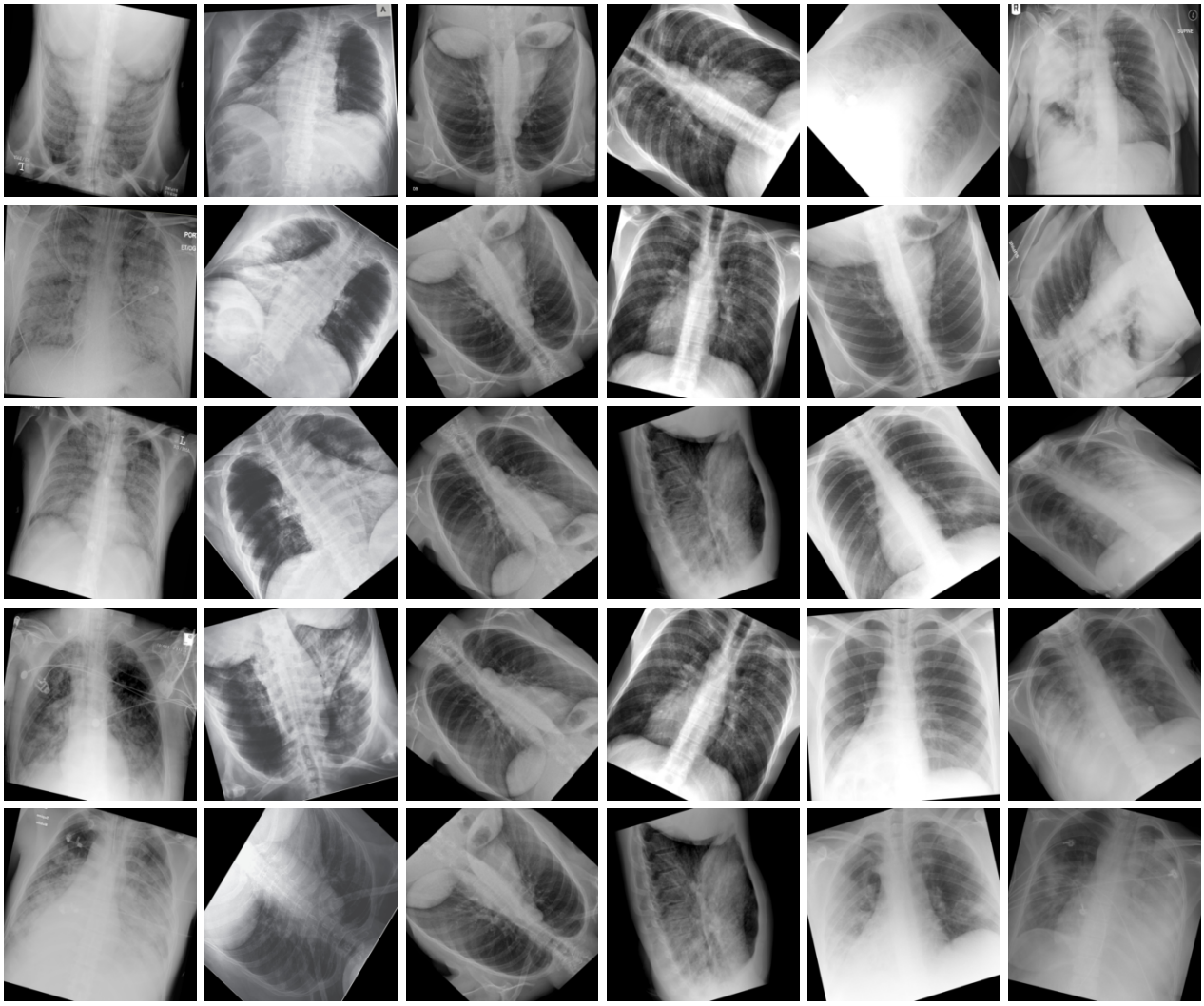

(a) (b) (c) (d) (e) (f)

Fig. 3: Several examples of training samples from (a) ARDS, (b) COVID-19, (c) No Finding, (d) Penumocystis, (e) SARS, and (f) Streptococcus classes.

DenseNet-121, we build COVID-19Net using four dense blocks on 224×224 input images. Before the first dense block, we use a convolutional layer followed by a pooling layer. The convolutional layer consists of $2k$ stride 2 convolutions, each with 7×7 of size. For the value of k, we follow the setting in DenseNet-121; $k = 32$. The last dense block is followed by a 7×7 global average pooling layer. To avoid over-fitting, we then place a drop-out layer with 0.5 of the drop rate and a batch normalization layer. Finally, we feed the features map to a classification layer that comprises a 6D fully connected layer with a softmax activation function.

C. Data Preparation

The CXR images with the corresponding class labels are provided by [21] that are made available at https://github.com/ieee8023/covid-chestxray-dataset. The dataset consists of 123 CXR images that belong to 6 classes, namely 'ARDS' (4 images), 'COVID-19' (99 images), 'No Finding' (1 image), 'Pneumocystis' (2 images), 'SARS' (11 images), and 'Streptococcus' (6 images). Since most class labels in the dataset, particularly for the 'No Finding' and 'Pneumocystis' classes, consist of relatively a small number of images, it may be difficult to ensure the generalization ability of COVID-19Net. To remedy this problem, we perform data augmentation, meant as producing additional examples by applying (generally randomized) transformations to the existing data. In our study, we apply random image rotation and translation operations on the images, such that for each image in the dataset, 15 new augmented images are generated. We perform the rotation and translation operations with the range of $\{\theta| -60 \leq \theta \leq 60\}$ and $\{x, y| -20 \leq x, y \leq 20\}$, respectively. From the augmentation process, we could generate 1845 new images altogether. Figure 3 shows several examples of the training samples.

D. Training Procedures

To train and test COVID-19Net, we need to split the augmented images into the training, validation, and testing datasets. However, no division initially made by the authors of the dataset [21]. Hence, we use the 10-fold cross-validation to carry out the training, validation, and testing procedures of COVID-19Net. For each fold, the proposed

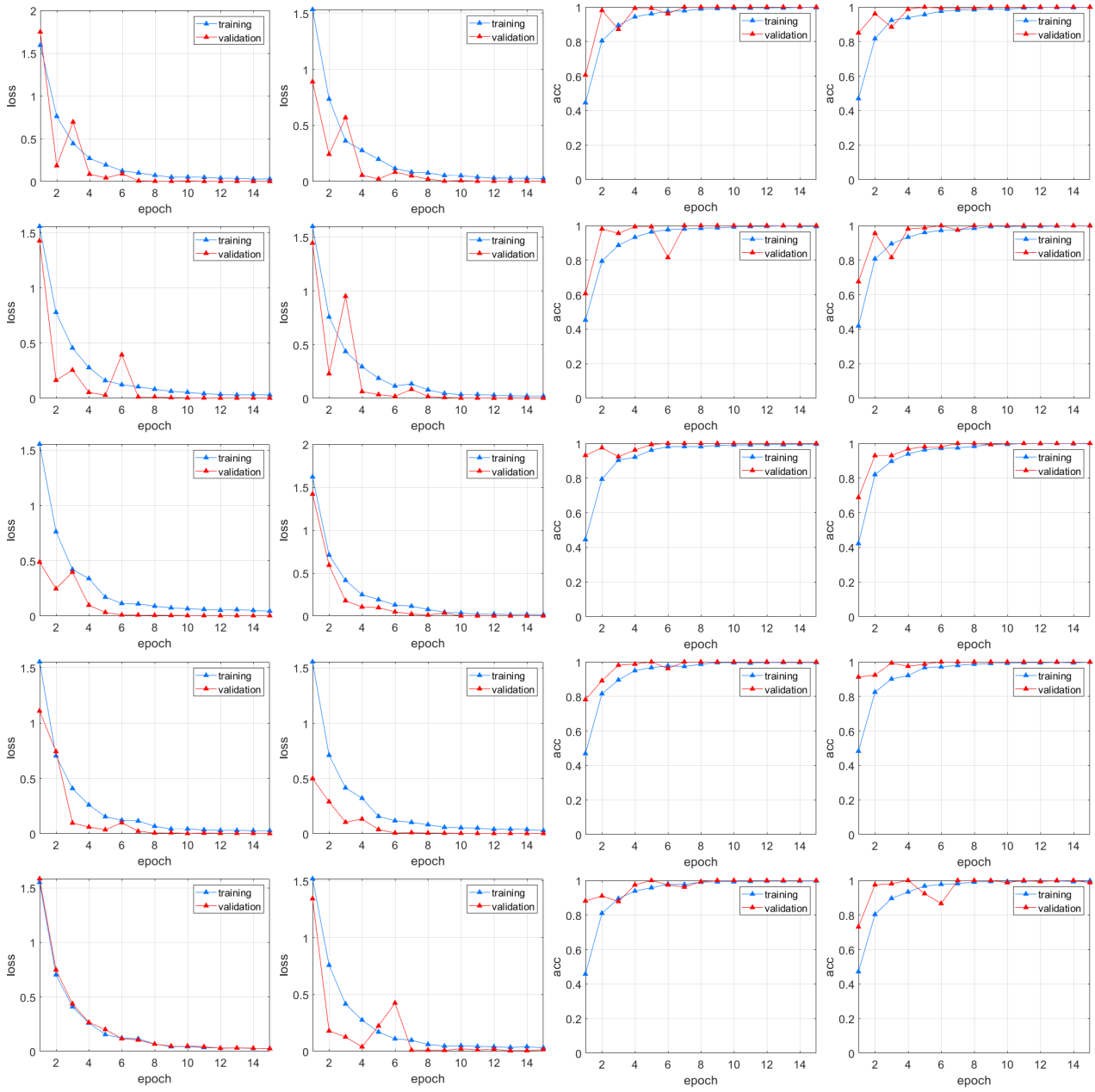

Fig. 4: The training-validation (a) losses and (b) accuracies of COVID-19Net. First and second columns in each of (a) and (b) are for training and validation performance on folds 1 to 5 and folds 6 to 10, respectively.

network is trained and validated on 90% of the augmented images using the Adam optimizer, mini-batch size of 10, and learning rate of 10^{-4} for 15 epochs. The remaining images are then used to test the trained COVID-19Net. The testing accuracy of COVID-19Net is calculated as the average of accuracies of all folds.

III. Experimental Results and Discussion

A. Training and Validation

We conduct our experiments on a CPU with Intel Xeon Processors @2.30 GHz and a GPU with an NVIDIA Tesla T4 card provided by Google Colaboratory. The machines require approximately 10 minutes to finish the training and validation processes on each fold. The COVID-19Net performance during the training procedure is illustrated by the accuracy and loss graphs in Figure 4.

From the figure, we may observe that COVID-19Net could achieve perfect validation accuracies on most folds. This fact suggests that the proposed network learns sufficient features, mainly due to its deep configuration. Moreover, it is interesting to note that no over-fitting spotted during the training processes. It indicates that our augmentation strategy could provide sufficient data for COVID-19Net to build a satisfactory generalization ability. Besides, the use of Over-fitting Combatant Layer may help the proposed network to avoid over-fitting.

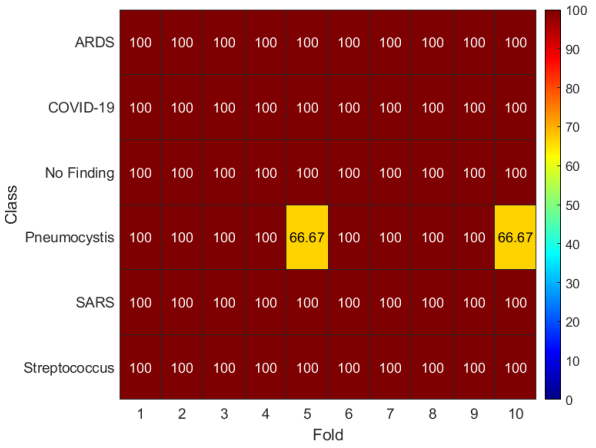

Fig. 5: Classification results of COVID-19Net.

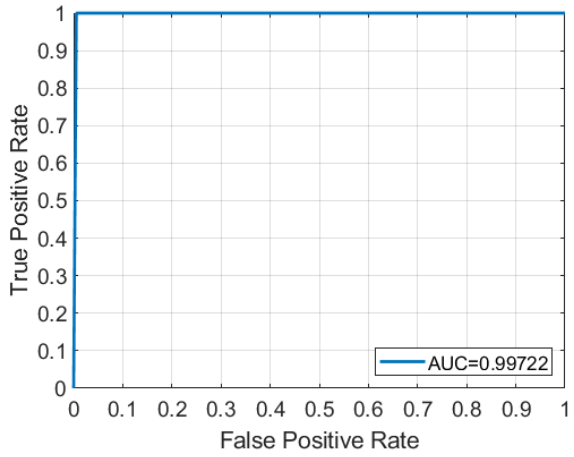

Fig. 6: The ROC curve of COVID-19Net on the two classes classification problem.

B. Classification Results

The classification results of COVID-19Net are presented in Figure 5. In the figure, we show the accuracy on each fold achieved by COVID-19Net. From the graphs, we may observe that the proposed network could classify all CXR images with COVID-19 indications to the correct class. The wrong classification happens only on two data with Pneumocystis indications. Since our main interest is to build an algorithm for COVID-19 diagnosis, it may be beneficial to investigate the performance of our network only in two-class labels, namely 'COVID-19' and 'Non COVID-19'. In this case, we may combine all classes other than 'COVID-19' into a single class 'Non COVID-19'. The ROC curve in Figure 6 illustrates the result of such an investigation. From the figure, it is observed that COVID-19Net achieves an almost perfect area under the ROC curve (AUC = 0.9972), indicating our proposed network could maintain excellent detection of COVID-19 with only a small number of false positives. In this respect, our algorithm would be beneficial for practical applications.

IV. Conclusion

In this paper, we have proposed COVID-19Net, a deep neural network-based algorithm to assist doctors in diagnosing COVID-19. The algorithm takes the CXR images in automatically diagnosing COVID-19. In the experimental parts, our algorithm could maintain an average classification accuracy of $> 99\%$ in diagnosing the viral COVID-19 and other related diseases like SARS, Streptococcus, ARDS, and Pneumocystis. While being used on the two classes classification problem, namely 'COVID-19' and 'Non COVID-19', COVID-19Net maintains an almost perfect area under the ROC curve (AUC = 0.9972), indicating our network could provide an ideal diagnosis of COVID-19 with only a small number of false positives. For future works, in developing COVID-19 screening frameworks, it would be desirable to include visualization techniques, such as Grad-CAM and occlusion sensitivity that are capable of explaining the diagnosis results provided by COVID-19Net.

References

[1] M.-Y. Ng, E. Y. Lee, J. Yang, F. Yang, X. Li, H. Wang, M. M.-s. Lui, C. S.-Y. Lo, B. Leung, P.-L. Khong, C. K.-M. Hui, K.-y. Yuen, and M. D. Kuo, "Imaging profile of the covid-19 infection: Radiologic findings and literature review," *Radiology: Cardiothoracic Imaging*, vol. 2, no. 1, p. e200034, 2020. [Online]. Available:

[2] T. Ai, Z. Yang, H. Hou, C. Zhan, C. Chen, W. Lv, Q. Tao, Z. Sun, and L. Xia, "Correlation of chest ct and rt-pcr testing in coronavirus disease 2019 (covid-19) in china: A report of 1014 cases," *Radiology*, vol. 0, no. 0, p. 200642, 0, pMID: 32101510. [Online]. Available:

[3] Y. Fang, H. Zhang, J. Xie, M. Lin, L. Ying, P. Pang, and W. Ji, "Sensitivity of chest ct for covid-19: Comparison to rt-pcr," *Radiology*, vol. 0, no. 0, p. 200432, 0, pMID: 32073353. [Online]. Available:

[4] G. Huang, Z. Liu, and K. Q. Weinberger, "Densely connected convolutional networks," *2017 IEEE Conference on Computer Vision and Pattern Recognition (CVPR)*, pp. 2261–2269, 2016.

[5] S. Ren, K. He, R. Girshick, and J. Sun, "Faster r-cnn: Towards real-time object detection with region proposal networks," *IEEE Transactions on Pattern Analysis and Machine Intelligence*, vol. 39, no. 6, pp. 1137–1149, 2017.

[6] J. Redmon, S. Divvala, R. Girshick, and A. Farhadi, "You only look once: Unified, real-time object detection," in *2016 IEEE Conference on Computer Vision and Pattern Recognition (CVPR)*, 2016, pp. 779–788.

[7] K. He, G. Gkioxari, P. Dollr, and R. Girshick, "Mask r-cnn," in *2017 IEEE International Conference on Computer Vision (ICCV)*, 2017, pp. 2980–2988.

[8] A. Krizhevsky, I. Sutskever, and G. E. Hinton, "Imagenet classification with deep convolutional neural networks," in *Advances in Neural Information Processing Systems 25*, F. Pereira, C. J. C. Burges, L. Bottou, and K. Q. Weinberger, Eds. Curran Associates, Inc., 2012, pp. 1097–1105. [Online]. Available:

[9] C. Szegedy, W. Liu, Y. Jia, P. Sermanet, S. Reed, D. Anguelov, D. Erhan, V. Vanhoucke, and A. Rabinovich, "Going deeper with convolutions," in *Proceedings of the IEEE Computer Society Conference on Computer Vision and Pattern Recognition*, vol. 07-12-June. IEEE Computer Society, oct 2015, pp. 1–9.

[10] K. He, X. Zhang, S. Ren, and J. Sun, "Deep residual learning for image recognition," in *2016 IEEE Conference on Computer Vision and Pattern Recognition (CVPR)*, 2016, pp. 770–778.

[11] K. Simonyan and A. Zisserman, "Very deep convolutional networks for large-scale image recognition," *arXiv preprint arXiv:1409.1556*, 2014.

[12] J. Long, E. Shelhamer, and T. Darrell, "Fully convolutional networks for semantic segmentation," in *2015 IEEE Conference on Computer Vision and Pattern Recognition (CVPR)*, 2015, pp. 3431–3440.

[13] O. Ronneberger, P. Fischer, and T. Brox, "U-Net: Convolutional Networks for Biomedical Image Segmentation," in *Medical Image Computing and Computer-Assisted Intervention MICCAI 2015. Lecture Notes in Computer Science*, F. A. Navab N., Hornegger J., Wells W., Ed. Springer, 2015, vol. 9351, pp. 234–241.

[14] P. Liskowski and K. Krawiec, "Segmenting Retinal Blood Vessels With Deep Neural Networks," *IEEE Transactions on Medical Imaging*, vol. 35, no. 11, pp. 2369–2380, 2016.

[15] L.-C. Chen, G. Papandreou, F. Schroff, and H. Adam, "Rethinking atrous convolution for semantic image segmentation," *ArXiv*, vol. abs/1706.05587, 2017.

[16] D. A. Dharmawan, D. Li, B. P. Ng, and S. Rahardja, "A new hybrid algorithm for retinal vessels segmentation on fundus images," *IEEE Access*, vol. 7, pp. 41 885–41 896, 2019.
[17] Q. Jin, Z. Meng, T. D. Pham, Q. Chen, L. Wei, and R. Su, "DUNet: A deformable network for retinal vessel segmentation," *Knowledge-Based Systems*, vol. 178, pp. 149–162, 2019. [Online]. Available:
[18] D. Li, D. A. Dharmawan, B. P. Ng, and S. Rahardja, "Residual u-net for retinal vessel segmentation," in *2019 IEEE International Conference on Image Processing (ICIP)*. IEEE, 2019, pp. 1425–1429.
[19] K. He, X. Zhang, S. Ren, and J. Sun, "Deep Residual Learning for Image Recognition," in *2016 IEEE Conference on Computer Vision and Pattern Recognition (CVPR)*, 2016, pp. 770–778.
[20] G. Larsson, M. Maire, and G. Shakhnarovich, "Fractalnet: Ultra-deep neural networks without residuals," *ArXiv*, vol. abs/1605.07648, 2016.
[21] J. P. Cohen, P. Morrison, and L. Dao, "Covid-19 image data collection," *arXiv 2003.11597*, 2020. [Online]. Available: